Design and evaluation of a continuous-wave diffuse optical tomography system

A. M. Siegel

Electro-Optics Technology Center, Tufts University, Medford, MA 02155
siegel@ll.mit.edu

J. J. A. Marota* and D. A. Boas

NMR Center and the Dept. of Anesthesia and Critical Care, Massachusetts General Hospital, Harvard Medical School, Massachusetts General Hospital East, Bldg #149, Charlestown, MA 02129*
dboas@nmr.mgh.harvard.edu

Abstract: Diffuse optical tomography (DOT) can image spatial variations in highly scattering optical media. We have built an inexpensive and portable continuous-wave DOT system containing 18 laser diode sources (9 at 780nm and 9 at 830nm) and 16 silicon detectors, which can acquire 288 independent measurements in less than 4 seconds. These data can then be processed using a variety of imaging algorithms. We first discuss the design of diffuse imaging equipment in general, and then describe our instrument, along with the technical issues that influenced its design. The technical challenges involved in performing DOT over large optode areas are discussed. We also present rat brain measurements following electrical forepaw stimulation using DOT. These results clearly demonstrate the capabilities of DOT and set the stage for advancement to quantitative functional brain imaging.

OCIS codes: (170.6960) Tomography; (170.5280) Photon migration

References and links

1. A. Yodh and B. Chance, "Spectroscopy and imaging with diffusing light," Phys. Today **48**, 34-40 (1995).
2. S. R. Arridge and J. C. Hebden, "Optical Imaging in Medicine: II. Modelling and reconstruction," Phys. Med. Bio. **42**, 841-854 (1997).
3. J. C. Hebden, S. R. Arridge and D. T. Delpy, "Optical imaging in medicine: I. Experimental techniques," Phys. Med. Bio. **42**, 825-840 (1997).
4. P. T. Fox and M. E. Raichle, "Focal physiological uncoupling of cerebral blood flow and oxidative metabolism during somatosensory stimulation in human subjects," Proc. Natl. Acad. Sci. USA **83**, 1140-4 (1986).
5. K. K. Kwong, J. W. Belliveau, D. A. Chesler, I. E. Goldberg, R. M. Weisskoff, B. P. Poncelet, D. N. Kennedy, B. E. Hoppel, M. S. Cohen, R. Turner, H.-M. Cheng, T. J. Brady and B. R. Rosen, "Dynamic magnetic resonance imaging of human brain activity during primary sensory stimulation," Proc. Natl. Acad. Sci. USA **89**, 5675-9 (1992).
6. S. Ogawa, T. M. Lee, A. R. Kay and D. W. Tank, "Brain magnetic resonance imaging with contrast dependent on blood oxygenation," Proc. Natl. Acad. Sci. USA **87**, 9868-72 (1990).
7. S. Ogawa, D. Tank, R. Menon, J. Ellermann, S.-G. Kim, H. Merkel and K. Ugurbil, "Intrinsic signal changes accompanying sensory stimulation: Functional brain mapping with magnetic resonance imaging," Proc. Natl. Acad. Sci. USA **89**, 5951-5955 (1992).
8. R. L. Barbour, H. L. Graber, J. Chang, S. S. Barbour, P. C. Koo and R. Aronson, "MRI-guided optical tomography:prospects and computation for a new imaging method," IEEE Computation Science and Engineering **2**, 63-77 (1995).
9. B. W. Pogue and K. D. Paulsen, "High-resolution near-infrared tomographic imaging simulations of the rat cranium by use of a priori magnetic resonance imaging structural information," Opt. Lett. **23**, 1716-1718 (1998).
10. B. W. Pogue, M. Testorf, T. McBride, U. Osterberg and K. Paulsen, "Instrumentation and design of a frequency-domain diffuse optical tomography imager for breast cancer detection," Opt. Express **1**, 391-403 (1997). http://epubs.osa.org/oearchive/source/2827.htm
11. N. Ramanujam, C. Du, Y. Ma and B. Chance, "Sources of phase noise in homodyne and heterodyne phase modulation devices used for tissue oximetry studies," Rev. Sci. Instru. **69**, 3042-3054 (1998).
12. B. Chance, M. Cope, E. Gratton, N. Ramanujam and B. Tromberg, "Phase measurement of light absorption and scattering in human tissues," Rev. Sci. Instru. **689**, 3457-3481 (1998).

#9224 - $15.00 US Received March 08, 1999; Revised March 30, 1999

13. P. N. den Outer, T. M. Nieuwenhuizen and A. Lagendijk, "Location of objects in multiple-scattering media," J. Opt. Soc. Am. A **10**, 1209-1218 (1993).
14. D. A. Boas, M. A. O'Leary, B. Chance and A. G. Yodh, "Scattering of diffuse photon density waves by spherical inhomogeneties within turbid media: analytic solution and applications," Proc. Natl. Acad. Sci. USA **91**, 4887-4891 (1994).
15. M. S. Patterson, B. Chance and B. C. Wilson, "Time resolved reflectance and transmittance for the non-invasive measurement of tissue optical properties," Appl. Opt. **28**, 2331-2336 (1989).
16. M. A. O'Leary, D. A. Boas, B. Chance and A. G. Yodh, "Refraction of diffuse photon density waves," Phys. Rev. Lett. **69**, 2658-2661 (1992).
17. J. B. Fishkin and E. Gratton, "Propagation of photon density waves in strongly scattering media containing an absorbing 'semi-infinite' plane bounded by a straight edge," J. Opt. Soc. Am. A **10**, 127-140 (1993).
18. A. Villringer and B. Chance, "Non-invasive optical spectroscopy and imaging of human brain function," Trends Neurosci **20**, 435-442 (1997).
19. G. Gratton, M. Fabiani, P. M. Corballis, D. C. Hood, M. R. Goodman-Wood, J. Hirsch, K. Kim, D. Friedman and E. Gratton, "Fast and localized event-related optical signals (EROS) in the human occipital cortex: comparisons with the visual evoked potential and fMRI.," NeuroImage **6**, 168-180 (1997).
20. B. Chance, A. Endla, N. Shoko, Z. Shuoming, H. Long, K. Worden, C. Li, T. Murray, Y. Ovetsky, D. Pidikiti and R. Thomas, "A novel method for fast imaging of brain function, non-invasively, with light," Opt. Express **2**, 411-423 (1998). http://epubs.osa.org/oearchive/source/4445.htm
21. M. Kohl, U. Lindauer, U. Dirnagl and A. Villringer, "Separation of changes in light scattering and chromophore concentrations during cortical spreading depression in rats," Opt. Lett. **23**, 555-557 (1998).
22. J. B. Mandeville, J. J. A. Marota, B. E. Kosofsky, J. R. Keltner, R. Weissleder, B. R. Rosen and R. M. Weisskoff, "Dynamic functional imaging of relative cerebral blood volume during rat forepaw stimulation," MRM **39**, 615-624 (1998).
23. J. B. Mandeville, J. J. A. Marota, C. Ayata, M. A. Moskowitz, R. M. Weisskoff and B. R. Rosen, "An MRI Measurement of the Temporal Evolution of Relative CMRO2 During Rat Forepaw Stimulation," Magn. Reson. Med. **In Review**, (1999).
24. J. J. A. Marota, C. Ayata, M. A. Moskowitz, R. M. Weisskoff, B. R. Rosen and J. B. Mandeville, "Investigation of the Early Response to Rat Forepaw Stimulation," Magn. Reson. Med. **In Press**, (1999).
25. A. C. Kak and M. Slaney, *Principles of Computerized Tomographic Imaging* (IEEE Press, New York, 1988).
26. M. A. O'Leary, D. A. Boas, B. Chance and A. G. Yodh, "Experimental images of heterogeneous turbid media by frequency-domain diffusing-photon tomography," Opt. Lett. **20**, 426-428 (1995).

1. Introduction

Diffuse Optical Tomography offers the capability to simultaneously quantify the tissue concentration of both oxy- (HbO) and deoxy-hemoglobin (Hb) [1-3]. Two or more near-infrared sources, with wavelengths specifically chosen to straddle the isosbestic point of the oxy/deoxyhemoglobin absorption spectrum, illuminate the tissue at various locations. The flux distribution at the tissue surface thus contains both spectral and spatial information about subsurface absorbers.

fMRI uses the paramagnetism of the Hb molecule to monitor metabolic activity through local changes in Hb, and thus blood oxygenation, hence the origin of the term BOLD (Blood Oxygen Level Dependent) imagery [4-7]. fMRI offers millimeter spatial resolution, but only the relative quantity of Hb is measured. DOT can simultaneously image changes in total hemoglobin concentration (which relates to blood volume) and oxygen saturation (HbO/(HbO+Hb)). One disadvantage of DOT is its limited spatial resolution, which leads to an intriguing possibility: the coregistration of simultaneously acquired DOT and functional MRI imagery, combining the spatial resolution of fMRI with the spectral discrimination of DOT [8, 9]. We plan to pursue such measurements in the near future with the instrumentation described in this manuscript.

In this paper, we discuss the engineering issues involved in the design of diffuse imaging equipment [10-12]. We then describe the design and evaluation of a continuous-wave (CW) DOT system that can image brain function in animals and humans with 4-second temporal resolution. We then present preliminary results showing that DOT is capable of quantitatively imaging both HbO and Hb concentration changes during brain activation in a rat model.

#9224 - $15.00 US Received March 08, 1999; Revised March 30, 1999

2. Background

Ballistic photon imaging is usually performed in a shot noise-limited, photon-starved environment due to the low percentage of photons that actually penetrate the tissue unscattered. Thus the photon-counting detectors require only a modest dynamic range. Diffuse imaging, on the other hand, employs many sources and detectors distributed over a large region of illuminated tissue, so each detector may operate over an effective photon path length ratio in excess of 10:1. With total optode source-detector geometries spanning less than 1cm, as in rat brain studies, this effect is negligible, and the hardware can easily accommodate the 60-80dB of dynamic range required for rather good quality imagery. On large subjects such as neonates or adult humans, however, optode dimensions of between 4 and 8cm are required. Under these conditions, that same photon path length ratio of 10:1 now translates into a flux attenuation range on the order of 10^6:1! In order to obtain all the information available, each detector must be capable of operating over a 120dB dynamic range, which is rather large from an electronic perspective. Although many techniques have been developed to solve this problem, all of them require a large capital investment in dollar cost and an increase in both measurement time and hardware complexity.

In order to collect enough photons to reach 120dB, the source power must increase and the detection noise must decrease. The source power will ultimately be limited in human patients by regulatory issues or, in experimental settings, by the vasodynamic effects of tissue heating, or in some cases, thermal necrosis. The detection noise floor can be reduced by improving the detectors and circuitry, but only to a point. Once the electrical noise contribution is reduced below the noise introduced by the fundamental uncertainty in the photon arrival rate, the system has become photon noise-limited or "background–limited". The only way to further reduce the noise level is to improve the statistics by increasing the total number of photons collected during each detector sample – which, for a fixed photon arrival rate, means a longer dwell time. This noise reduction is proportional to the square root of the total number of photons collected, and hence to the square root of the total photon collection time. Thus, a fundamental tradeoff exists between measurement time and dynamic range.

If sufficient power and measurement time is available and a signal can be detected, the next challenge begins: what to do with these signals and how to keep them clean. Direct digitization of a 120dB signal would require a 22 bit A/D converter, although logarithmic compression may reduce this to a far more practical 16 bits. Now that the signals can be detected and digitized, the entire system must be capable of preserving their quality. This means that detector channel-to-channel crosstalk, multiplexer settling, and feedthru should be around –120dB. This can best be achieved by performing the A/D conversion directly following detection. Electromagnetic interference, power, and ground isolation all must approach the quantization limit – about half a DN (Digital Number) or so. All of these requirements can be met, but it would require a carefully constructed system based upon a well-engineered design.

Many other, perhaps better, solutions exist - such as using two or more lower dynamic range fixed-gain detectors at each optode location, or perhaps using a switch to reduce the detector gain by known increments when a certain signal voltage threshold is exceeded. All of these still require the same level of attention to signal quality and integrity as discussed above.

Diffuse imaging techniques can be grouped into two general categories: "scalar" and "vector" techniques:

Scalar techniques measure the optical flux exiting the tissue. The system we describe below is a scalar system. There is additional useful information available in the form of the average photon path length. Some light travels deeply into the tissue and returns to the surface, most of the light passes through the classic banana-shaped region, and a small amount travels the shortest path between the source and the detector. A localized absorption at a specific depth will attenuate only the small number of photons which pass through that region, leaving the rest unaffected [13, 14]. Since the average photon path length, and thus the transit

#9224 - $15.00 US Received March 08, 1999; Revised March 30, 1999

time, varies significantly with depth, the magnitude of the photon flux versus the average photon transit time provides a measure of the relative absorption vs. tissue depth – a valuable piece of information. (Although most in-vivo imaging - especially brain imaging - requires light to travel through various tissue types: skin, bone, cerebrospinal fluid, etc., and the resulting optical heterogeneity complicates image reconstruction, these basic concepts still apply).

Vector techniques measure both the magnitude and the average propagation delay, either directly, or in the form of amplitude and phase-shifts relative to the modulation frequency of the light source. Two common vector approaches in use today are the *time-domain* approach [15] and the *frequency-domain* approach [11, 16, 17]. A time-domain system employs picosecond-wide optical pulses, time-gated photon-counting detectors, time-to-amplitude converters, and the like. Typical frequency-domain systems use a radiofrequency (RF) modulated light source, photomultiplier tubes or fast photodiodes feeding tuned RF amplifiers, and an RF inphase/quadrature (I/Q) phase detector followed by postdetection filters.

Although time-domain systems are flexible and can detect both ballistic and diffusely scattered photons, they are expensive and, due to their wideband nature, require significant averaging in the digital domain to improve the signal-to-noise ratio (SNR). Frequency-domain systems use simpler, lower-cost components and provide greater SNR. The simplicity and cost savings result from the widespread commercial availability of excellent RF circuitry at modest cost, specifically around common satellite and radar receiver intermediate (IF) frequencies such as 70MHz, 140MHz, 200MHz, etc. The greater SNR stems from the fact that, unlike the wideband nature of time-domain measurements, frequency-domain measurements are usually performed at single RF frequencies, so they occupy a much narrower bandwidth. In the ideal case, the detector electronics need only occupy an RF bandwidth commensurate with about twice the signal acquisition rate (to capture both sidebands), much as the coherent detection system described below. Although this may be impractical due to component instabilities, bandwidths in the Hz to low kHz range are quite practical.

Regardless of the techniques employed, all DOT instrumentation should be designed with the following parameters in mind: Large optode separations lead to significant optical attenuation, so multiple optode spacings will require a **large dynamic range**. The system should be as **linear** as possible over this dynamic range in order to keep the measurements both accurate and precise. **Stray light rejection** is important for systems that must operate outside of the sheltered confines of the laboratory, especially in clinical settings, which often contain large amounts of "optical pollution". Both optical and electrical **crosstalk** should be reduced to levels commensurate with the system dynamic range, if possible. Good **long-term stability** means fewer and less frequent calibration cycles, and good **temporal response** is important for functional imaging, however it comes at the cost of an increase in the noise floor, which reduces dynamic range.

3. The prototype CW DOT system

Our goal was to develop a prototype portable diffuse imager which can be used as a research tool for both characterizing tissue optical properties and guiding us toward future hardware and software design improvements. For simplicity, we decided on a magnitude-only system. Our optical sources were standard low-power laser diodes. Although more powerful light-emitting diodes were available, coupling that light into the various core sizes of both plastic and glass fiber would have been very difficult and far less optically efficient. Our detector options ranged from multianode PMTs to discrete commercial-grade photodiodes with external preamplifiers. We compromised by choosing a monolithic photodiode/preamplifier IC housed in a clear 8-pin DIP package (OPT209 from Burr-Brown, Tucson, AZ). This offered both the convenience and low-cost of a solid-state detector, combined with the electrical and optical isolation of an integrated preamplifier. Although the parasitic capacitances of the monolithic preamp were about twice that of a well-designed discrete circuit, the simplicity and the less stringent electrical shielding requirements for the monolithic preamp swayed our decision.

#9224 - $15.00 US Received March 08, 1999; Revised March 30, 1999

Our goal was to achieve a useable dynamic range of at least 80dB. Dynamic range and linearity are closely paired, since each must be defined with reference to the other. For example, a statement of a given dynamic range value is, in itself, meaningless unless the criteria for determining the limits of that range are expressly stated. In our case, our goal was 80dB of dynamic range with less than a 1% deviation from a least-squares-fit line. Although this linearity value was somewhat arbitrarily selected, it gave us a good starting point around which to base our design. Since valuable information can often be gleaned even from saturated signals, we decided to "bracket" the signal swing within the dynamic range of our A/D converter.

In order to meet the 80dB objective, crosstalk, drift, settling time, and feedthru errors had to match this goal. Optical crosstalk was minimized by concealing each detector package in opaque heatshrink tubing and providing sufficient separation to further attenuate any stray reflections within the metal housing. Each detector fiber was sheathed in opaque tubing as well, which also served to protect the fragile cladding of the PMMA (acrylic) fibers from abrasion. Electrical crosstalk occurring at the front end was not significant since the only high impedance node in the preamp was physically removed from the DIP package and the modulation frequency was in the kilohertz range. Ground loops were minimized by using an electrically isolated power supply, a battery-powered portable laptop computer, and a single-point earth connection to safety ground. Crosstalk through power lines was minimized with on-board regulation and the use of separate power supply decoupling filters at each opamp. To reduce settling time errors, we planned for a 5τ dwell time prior to conversion. For a post-detection time constant of 40ms, this gave us a minimum delay of 200ms per source. Faster acquisition rates could easily be achieved, albeit at the cost of higher crosstalk. Feedthru among multiple channels within the analog multiplexer was minimized by switching only demodulated (baseband) signals and by reducing the DC currents through the switches by placing a buffer directly at the multiplexer output. This also provided better linearity, since switch impedance varies with common-mode voltage.

We chose to use a rather fast 133 kilosample-per-second, 16 bit A/D converter (Analog Devices AD7884) for a number of reasons. The high sample rate allowed us to rapidly scan through the 16 demodulated outputs during high data rate measurements, while still permitting us to oversample and then average in the digital-domain during slower measurements. The parallel data output design made it easy to interface with all of the digital I/O boards used in our lab. A summary of our performance goals for the prototype DOT imager is shown in Table 1.

Since we planned to perform some measurements in a clinical setting, the unit had to operate within a normal hospital environment. This placed a severe stray-light rejection requirement on our design. We needed to detect picowatts of source signal under an ambient optical background in the microwatt range (as seen by the detector). We solved this problem by using synchronous detection.

#9224 - $15.00 US Received March 08, 1999; Revised March 30, 1999

Table 1. Our performance goals for the prototype DOT imager.

PARAMETER	GOAL
DYNAMIC RANGE	10,000:1 (80dB)
NONLINEARITY	<1% over the 80dB dynamic range
SETTLING TIME	<300ms to 0.1%
CROSSTALK	<0.01%
DIGITAL RESOLUTION	16 bits
SOURCE CHANNELS	9 at 780nm and 9 at 830nm
SOURCE OPTICAL POWER	~5mW
DETECTORS	16 Si photodiode/preamplifiers (OPT209)
MODULATION TECHNIQUE	single-phase squarewave AM with coherent detection
POSTDETECTION BANDWIDTH	10 to 20Hz
STRAY LIGHT REJECTION	<1% error under normal illumination levels
PACKAGING ISSUES	must be portable, compact, and extremely rugged
POWER REQUIREMENTS	120VAC +/-10%, 50-60Hz
PATIENT SAFETY	leakage current <1μA, case-to-gnd impedance <1Ω

Synchronous detection, is a technique which offers substantial advantages when detecting small signals buried in random, uncorrelated noise (with respect to the modulation frequency). In order for coherent detection to work, the source must be intensity-modulated in some known fashion, usually in the form of a 50% duty cycle squarewave or sinusoidal waveform, which we create by modulating the bias current through the laser diode sources. Each photodetector preamp output is first highpass filtered to remove low frequency signals from stable interference sources like sunlight and 1/f (flicker) noise generated by the electronics. The medium frequency components produced by fluorescent lamps at 120Hz and its harmonics are somewhat attenuated as well. This filtered preamp output is then fed into a double-balanced mixer. The mixer, which is gated by the same modulator that controls the laser diode source intensity, synchronously rectifies the weak modulated source signal, which appears as a small DC voltage at the mixer output. All other spurious modulated optical signals (including those produced by line-powered lamps, computer terminals, multiplexed LED displays, etc.) which are not phase-coherent to the source will exit the mixer in the form of frequency-shifted AC signals. A lowpass filter placed at the output of the mixer strongly attenuates these incoherent signals, leaving only the small DC voltage proportional to the magnitude of the source energy detected. The time constant of this lowpass filter controls the post-detection bandwidth, which significantly reduces the noise level, but also limits the rate at which the desired signal intensity changes can be detected. It is important to set this bandwidth as low as practical to minimize noise, since the noise is proportional to the square root of the post-detection bandwidth. The modulation frequency, which is typically between 100Hz and 100kHz, can be adjusted slightly to shift the detection passband away from narrowband interference sources that happen to fall near harmonics of the modulation frequency. These interference sources can sometimes generate intermodulation products (undesired signals created in the demodulation process, equal in frequency to the difference between the interference frequency and the modulation frequency or one of its harmonics) within the postdetection bandwidth, which are sometimes difficult to remove otherwise.

We used a nominal modulation of 2kHz, which was chosen to shift the detection band out to a frequency region where the flicker noise was low, yet to where the detector/preamps were still capable of responding to the third harmonic at 6kHz. Although third harmonic response

#9224 - $15.00 US Received March 08, 1999; Revised March 30, 1999

was not critical for operation, it served to improve the "average-to-peak" voltage ratio of the received signal, and so provided a little more dynamic range at the high end. The post-detection time constant was set at 40ms, and a dwell time of ~200ms was chosen to provide sufficient settling for each detector channel. This time constant was chosen to both provide significant noise reduction and yet remain fast enough to perform basic functional imaging studies.

Both source and detector selection were under direct computer control. This both simplified the digital design and offered us the flexibility to operate as few or as many sources and detectors as needed. A block diagram of the prototype DOT imager is shown in Figure 1 below.

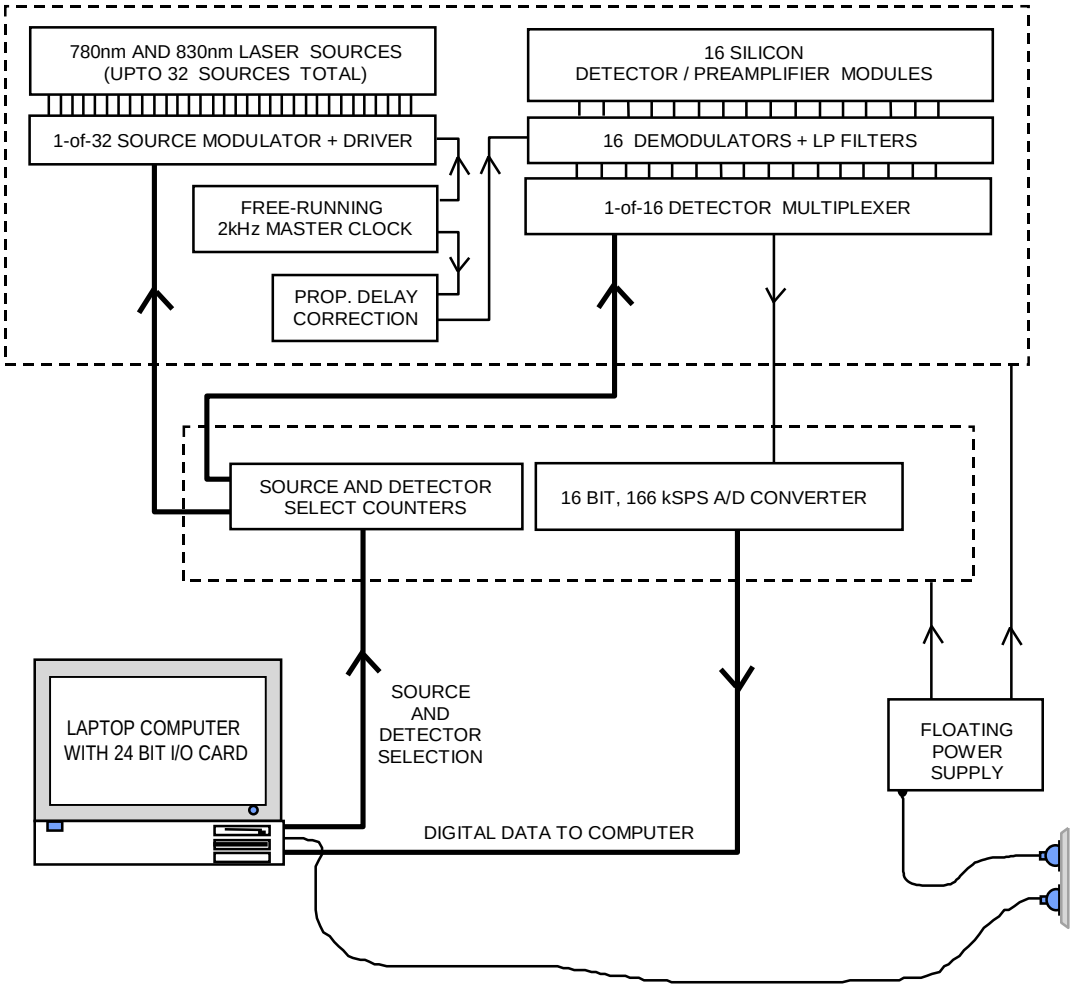

Fig. 1. A block diagram of the prototype DOT imager. All functions, including source and detector selection, are computer-controlled.

4. The DOT system performance evaluation

Our measurements revealed the overall system performance to be slightly better than expected. Crosstalk and stray light rejection were not the performance limiters, as had been feared. The lasers provided enough power to handle an optode geometry of 4cm x 6cm (for piglet studies), yet the detectors could handle a 1cm x 1.5cm geometry (for rat studies) without saturating.

#9224 - $15.00 US
Received March 08, 1999; Revised March 30, 1999

This meant that from a detector sensitivity standpoint, we guessed well. A summary of our test results is shown in Table 2 below.

Table 2. Results of the measurements performed on the prototype DOT imager.

PARAMETER	MEASURED VALUE
NOISE EQUIVALENT POWER	<40pW RMS (measured with 32 samples per dwell)
DYNAMIC RANGE	~45,000:1 (92dB) @ 0.75% nonlinearity ~25,000:1 (88dB) @ 0.05% nonlinearity
LONG-TERM STABILITY	+/-1% of reading in 30 minutes (half-scale output)
INTERCHANNEL CROSSTALK	<1:20,000 (-86dB)
STRAY LIGHT REJECTION	~1 DN signal change from darkness to normal ambient using cool-white fluorescent and incandescent lamps
TEMPORAL RESPONSE	~20Hz
POWER DELIVERED TO TISSUE	2mW @ 780nm, 8mW @ 830nm

The system noise floor was obtained by calculating the standard deviation of a number of readings taken at the lowest resolvable source intensity. The noise equivalent power was then calculated for an SNR of unity, using the power-per-unit-flux value obtained from the linearity measurement.

Dynamic range and linearity are related: the dynamic range can only be defined with reference to a specified linearity limit. This is why two dynamic range/linearity values were presented in Table 2 above. The incident beam from an optical source was sampled with a "monitor" fiber that led to a calibrated power meter. The linearity was then measured by comparing this value to the DOT instrument reading over a wide range of flux levels. The flux was varied using neutral density filters. A diffuser was used to reduce the spatial coherence of the source, which prevented modal noise in the fibers from interfering with the measurement.

Long-term stability was measured by noting the total drift between initial and final readings for a fixed probe geometry on a static phantom.

Interchannel crosstalk was measured as a single detector channel was alternately driven between the noise floor and full-scale output using the diffuser/ND filter technique described earlier. The largest level change among the other fifteen channels was recorded.

Stray light rejection was measured by operating the system with a static phantom in a dark room and then turning on both the fluorescent lights and a computer display located about a meter away. The largest change among the sixteen detector channels was recorded. The detected power in the visible band was ~1.5uW. The temporal response was defined by the bandwidth of the single-pole postdetection filters, which were set to 20Hz. This was not directly measured.

The power delivery was measured at the end of ~1 meter of 1mm dia. polymethyl methacrylate fiber using a calibrated power meter. No index-matching with the detector was attempted. This will underestimate the actual power by ~4% for in-vivo measurements due to index-matching from perspiration trapped at the fiber/skin interface.

5. Preliminary validation of DOT through in-vivo measurement of rat brain function

In order to evaluate the effectiveness of this design, we used this device to detect localized changes in cortical hemodynamics in response to a somatosensory evoked potential in an anesthetized rat. In this study, electrical stimulation was applied to the median nerve within the

#9224 - $15.00 US Received March 08, 1999; Revised March 30, 1999

forepaw; this is known to activate a volume of sensorimotor cortex within the parietal lobe. Any sensory stimulation (motor, sensory, visual, cognitive, etc.) produces a localized neuronal activation with a concomitant increase in metabolic rate. Because of flow-metabolism coupling, there is a localized increase in blood flow to fulfill the local increase metabolic demand for oxygen and glucose. The result is a localized increase in blood volume and, therefore, hemoglobin concentration. Because the increase in blood flow exceeds oxygen extraction, hemoglobin saturation also increases. This is the basis for the MRI signal change associated with the BOLD response and has been explored with diffuse optical techniques by a number of investigators [18-21].

With approval of the Massachusetts General Hospital Subcommittee on Animal Research Care, a male Harlan Sprague Dawley rat (approx. weight 400 grams) was anesthetized with 1.5% halothane in oxygen for surgical preparation including insertion of femoral arterial and venous catheters and tracheostomy.[22-24]. The rat was mechanically ventilated with a small animal ventilator (Harvard Apparatus) throughout the experiment. The halothane was discontinued and anesthesia was maintained with a 50 mg/kg intravenous bolus of alpha-chloralose followed by continuous intravenous infusion at 40 mg/kg/hr. In order to facilitate ventilation and to prevent muscular contractions from generating motion artifacts during stimulation, the rat was paralyzed with a 2mg/kg intravenous bolus of pancuronium followed by continuous intravenous infusion at 2 mg/kg/hr. Arterial blood pressure and rectal temperature were monitored throughout; body temperature was maintained at 37.5 ± 0.5C by means of a heating blanket. Arterial blood P_aO_2, P_aCO_2 and pH were determined from samples withdrawn through the arterial catheter; ventilation was adjusted to maintain normal values. Two thin copper wires were inserted just beneath the hide into the forepaw at the level of the carpal bones. Electrical stimulations were delivered as 5 volt square wave pulses of 0.5msec duration at a 3 Hz repetition rate. Prior to paralysis, this voltage was determined to be at least 2.5 times the level at which a muscular twitch response was generated.

The head was secured in a stereotactic head frame both to reduce motion artifacts and to serve as a mechanical support for a three-axis translation stage used to position the optode assembly directly against the scalp. The stimulation protocol consisted of acquisition of a baseline image immediately followed by a 45-second period of stimulation during which an image was acquired every 5 seconds. After stimulation was discontinued, images were collected every 5 seconds for an additional 60 seconds. All stimulations were performed at least 45 min after discontinuation of the halothane in order to permit time to recover from the volatile anesthetic.

The optode arrangement is shown in Figure 2. The 9 source fibers were arranged in a 3 x 3 grid with a 3 x 5 mm spacing. The 16 collection fibers were arranged in a 4 x 4 grid with the same 3 x 5 mm spacing. The 9 x 15 mm probe was designed and positioned to span the lateral extent of the brain. To improve optical coupling, the height of each fiber was manually adjusted to match the surface contours of the skull. The Z-positions were not measured, nor was the actual contour of the scalp. The images were reconstructed with the assumption that the scalp contour was flat and that the scalp, skull, cerebral spinal fluid, and brain system could be treated as a homogeneous, semi-infinite medium, except for the localized activation. Images were reconstructed in a 9 x 15 mm plane positioned at a depth of 4 mm, with a thickness of 1 mm, and located parallel to the source/detector plane. The voxel size was 0.45 x 0.75 x 1 mm. With this geometry, we only reconstruct 2D images of the absorption coefficient and we assume that the out-of-plane optical properties remain unchanged. This means that any out-of-plane optical changes that do occur are projected into the image plane. Our reconstructions were performed using 10 iterations of the SIRT algorithm, starting with an initial guess of zero perturbation [25, 26]. It was critical to phase-lock the image sequence with the respiration rate to minimize the physiologic interference due to periodic changes in venous volume due to positive pressure mechanical ventilation.

The results, presented here as an average of 6 trials on a single rat, are shown in the following figures. Figure 2 shows the results of a 45-second stimulation to the right forepaw.

#9224 - $15.00 US Received March 08, 1999; Revised March 30, 1999

The baseline image is shown at 0 seconds as well as the peak activation image at the end of the 45-second stimulation, followed by a return to the baseline image at 95 seconds. The images reveal an increase in absorption in the left hemisphere. A greater increase in the absorption coefficient was seen at 830nm compared to 780nm. This is consistent with the standard vascular response of increased blood volume and oxygen saturation.

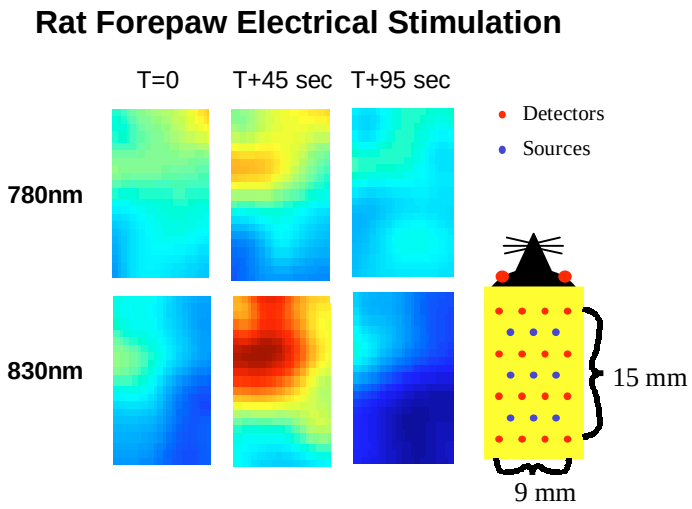

Fig. 2. DOT images of rat brain function at the peak response following 45 seconds of electrical forepaw stimulation. The recovery to baseline is shown 50 seconds following cessation of activation. Dark blue represents a change in the absorption coefficient of 0 cm^{-1} while dark red represents a change of 0.004 cm^{-1}.

6. Future systems under development

We are currently involved in the design of a number of systems ranging from general multipurpose imagers to specific purpose-built units. Based on the lessons learned during the development of the DOT imager described above, we have designed and are currently building an autonomous diffuse imager for optical mammography studies. This system will collect and store complete frames of data within an on-board memory module. Both the detector bandwidth and the sample rate are adjustable to optimize acquisition speed. We plan to double our acquisition rate by operating two lasers simultaneously and resolving the two signals using phase diversity. We are also developing a stroke monitoring system for humans, using four high power laser diode sources and discrete detectors, held close to the scalp to minimize fiber coupling and attenuation losses. Although all four lasers operate at the same wavelength, each source-detector pair will be isolated through a combination of phase diversity and tissue attenuation.

What is phase diversity? The prototype DOT imager could only energize one source at a time, which limited our acquisition rate. A more efficient technique is to exploit the phase diversity afforded by coherent detection by modulating each laser wavelength at the same 2kHz frequency but in phase quadrature with each other. Double-balanced mixers are insensitive to coherent signals that arrive exactly 90’ out of phase with the demodulation clock. When a quadrature signal passes through the mixer, the DC level of the resulting signal averages out to zero, similar to uncorrelated noise. The mixer, fed by a detector signal containing both in-phase and quadrature components (generated by the two laser sources), will demodulate the in-phase signal only, and will completely ignore the quadrature component. The same holds true for the second mixer, fed with a “quadrature” demod clock. Double-pole

#9224 - $15.00 US
Received March 08, 1999; Revised March 30, 1999

postdetection filters are used to attenuate the strong second harmonic component produced by the quadrature source.

There are some limitations to this technique, however. Interchannel isolation is critically dependent on accurate and stable phase control throughout the system. The good news is twofold: Since the propagation delay through most components varies little with voltage or temperature, long term stability is expected to be excellent. Our four-channel prototype system has maintained an interchannel isolation of more than 50dB for many months. Furthermore, since the *difference* between μ_a at 780nm and at 830nm is relatively small, the amplitude difference between the two signals is only around 10:1 (20dB), so an interchannel isolation of 40dB is more than adequate for our needs. Two disadvantages with this technique, however, are a reduction in dynamic range and a slight increase in the noise floor when using background-limited detectors (from the additional flux generated by the quadrature source). An example of such a system is shown by the schematic in Figure 3 below.

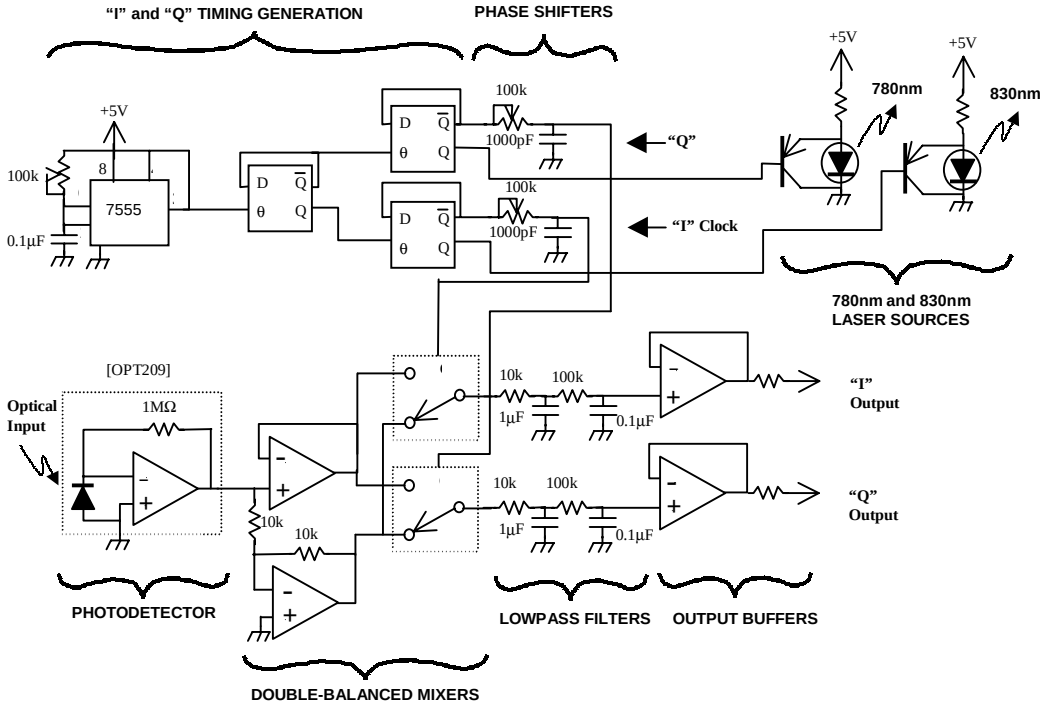

Fig 3. The schematic diagram of a single detector phase diversity prototype system. A four-channel version was developed to evaluate phase diversity in more complex two-wavelength systems.

7. Summary

Diffuse optical tomography (DOT) can image spatial variations in highly scattering media, and offers great promise as an adjunct to fMRI for simultaneous real-time quantification of total hemoglobin concentration and oxygen saturation. We discussed a number of issues that influence the design and development of diffuse imaging instrumentation. We then described the construction and testing of a prototype CW DOT imager, which was later used to acquire DOT images of rat brain function following forepaw stimulation. These DOT images qualitatively agree with the expected vascular response to neuronal activation. In particular, our measured absorption changes are consistent with the standard observation of an increase in blood volume and oxygen saturation.

#9224 - $15.00 US Received March 08, 1999; Revised March 30, 1999

8. Acknowledgements

We gratefully acknowledge the financial support from the National Institutes of Health 1R29NS37053-01 and from the Center for Innovative Minimally Invasive Therapies. We would also like to thank Edward Smolinsky for his help in constructing the DOT imager.

#9224 - $15.00 US Received March 08, 1999; Revised March 30, 1999